



Published in final edited form as:

ACS Infect Dis. 2020 May 08; 6(5): 1214–1227. doi:10.1021/acsinfecdis.0c00015.

Identifying OXA-48 Carbapenemase Inhibitors Using DNA-Encoded Chemical Libraries

Doris Mia Taylor[†], Justin Anglin^{‡,Φ}, Suhyeorn Park[‡], Melek N. Ucisik^{‡,Φ}, John C. Faver^{‡,Φ}, Nicholas Simmons^{‡,Φ}, Zhuang Jin^{‡,Φ}, Murugesan Palaniappan^{‡,Φ}, Pranavanand Nyshadham^{‡,Φ}, Feng Li^{‡,Φ,‡}, James Campbell^{‡,Φ}, Liya Hu[†], Banumathi Sankaran, B.V. Venkataram Prasad[†], Hongbing Huang^{‡,Φ,‡}, Martin M. Matzuk^{‡,Φ,‡}, Timothy Palzkill^{†,‡,*}

[‡]Center for Drug Discovery, Baylor College of Medicine, Houston, TX, 77030 USA

[†]Verna and Marrs McLean Department of Biochemistry and Molecular Biology, Baylor College of Medicine, Houston, TX, 77030, USA

^ΦDepartment of Pathology & Immunology, Baylor College of Medicine, Houston, TX, 77030, USA

[‡]Department of Pharmacology and Chemical Biology, Baylor College of Medicine, Houston, TX, 77030, USA

Berkeley Center for Structural Biology, Advanced Light Source, Lawrence Berkeley National Lab, CA, 94720, USA

Abstract

Bacterial resistance to β -lactam antibiotics is largely mediated by β -lactamases, which catalyze the hydrolysis of these drugs and continue to emerge in response to antibiotic use. β -lactamases that hydrolyze the last resort carbapenem class of β -lactam antibiotics (carbapenemases) are a growing global health threat. Inhibitors have been developed to prevent β -lactamase-mediated hydrolysis and restore the efficacy of these antibiotics. However, there are few inhibitors available for problematic carbapenemases such as Oxacillinase-48 (OXA-48). A DNA-encoded chemical library approach was used to rapidly screen for compounds that bind and potentially inhibit OXA-48. Using this approach, a hit compound, CDD-97, was identified with sub-micromolar potency ($K_i = 0.53 \pm 0.08 \mu\text{M}$) against OXA-48. X-ray crystallography showed that CDD-97 binds non-covalently in the active site of OXA-48. Synthesis and testing of derivatives of CDD-97 revealed structure-activity relationships and informed the design of a compound with a two-fold increase in potency. CDD-97, however, synergizes poorly with β -lactam antibiotics to inhibit the growth of bacteria expressing OXA-48 due to poor accumulation into *E. coli*. Despite the low *in vivo* activity, CDD-97 provides new insights into OXA-48 inhibition and demonstrates the

*Corresponding Author: Timothy Palzkill, Tel:(713)-798-5609; timothy@bcm.edu.

Supporting Information

The supporting information is available free of charge on the ACS Publications website. The following is provided in Supporting Information.

Accession Codes

The atomic coordinates and structure factors of the CDD-97/OXA-48 structure have been deposited at the Protein Data Bank under accession code 6UVK.

potential of using DNA-encoded chemistry technology to rapidly identify β -lactamase binders and to study β -lactamase inhibition, leading to clinically useful inhibitors.

Keywords

β -lactam antibiotic; β -lactamase; carbapenemase; OXA-48; drug discovery; DNA-encoded library; DECL; DEC-Tec

Multidrug-resistant bacteria are associated with 2 million infections and approximately 23,000 deaths per year in the U.S. alone and thus are a serious threat to public health¹. Growing resistance to the invaluable β -lactam antibiotic family is a concern that is elevated by the slowed development of novel therapeutic agents. β -lactam antibiotics make up approximately 65% of the prescribed antibiotics worldwide and reduced efficacy of these drugs due to resistance would severely impact the treatment of bacterial infections²⁻⁴. β -lactams act by covalently inhibiting essential cell wall biosynthesis transpeptidase enzymes called penicillin-binding proteins (PBPs), which leads to cell death^{5,6}. Bacteria can circumvent the bactericidal effect of β -lactams by expressing β -lactamase enzymes that hydrolyze the pharmacophoric β -lactam ring of the antibiotics to confer resistance⁷⁻⁹. β -lactamase inhibitors have been developed and used in conjunction with β -lactams to suppress β -lactamase activity and prolong antibiotic efficacy^{2,10}. However, nearly 5000 different β -lactamases have been identified¹¹ and the potency of inhibitors varies among enzymes. Inhibitor-resistant β -lactamases that hydrolyze the last resort carbapenem class of β -lactam antibiotics are a particular concern.

Carbapenem-resistant *Enterobacteriaceae* (CRE) infections are associated with increased patient morbidity and mortality and new treatment options are needed^{1,12,13}. The Gram-negative *Enterobacteriaceae* family frequently causes multidrug-resistant nosocomial infections and the presence of carbapenem-hydrolyzing β -lactamases, or carbapenemases, in these strains severely limits treatment options. Most β -lactamases are unable to hydrolyze carbapenems due to the unique stereochemistry of these antibiotics¹⁴. The emergence and dissemination of carbapenemases has resulted in increased β -lactamase-mediated resistance to the drugs^{13,15-17}.

β -lactamases are grouped into classes A – D based on primary amino acid sequence homology and enzyme mechanism. Classes A, C, and D inactivate β -lactam antibiotics through a serine hydrolase mechanism while members of class B are metalloenzymes that utilize zinc ions for hydrolysis^{18,19}. The most prevalent carbapenemases in *Enterobacteriaceae* are the class A KPC-2 β -lactamase, the NDM, IMP, and VIM enzymes of class B, and the class D enzyme OXA-48¹³. OXA-48 was first reported from a *Klebsiella pneumoniae* isolate in Turkey in 2008. However, it has now been identified worldwide in a range of *Enterobacteriaceae*. OXA-48 is resistant to all clinically available β -lactamase inhibitors except avibactam²⁰⁻²².

β -lactam-based molecules such as clavulanic acid were the first clinically available inhibitors and their ability to synergize with antibiotics proved an effective strategy to manage resistance¹⁰. Unfortunately, these inhibitors are largely ineffective on OXAs¹³ and

are susceptible to hydrolysis and resistance due to the β -lactam ring^{23–25}. Non- β -lactam-based inhibitors have the prospect of slowing β -lactamase-mediated resistance as new mechanisms of inhibitor inactivation will likely be required²⁶. Inhibitors that do not contain a β -lactam ring such as avibactam, relebactam (both diazabicyclooctanes) and vaborbactam (boronic acid-based) have unique scaffolds yet covalently inhibit a range of β -lactamases. Despite having variable activity against the Class D enzymes, avibactam is the only clinically available inhibitor with significant efficacy against OXA-48²¹. Relebactam and vaborbactam are ineffective against OXA-48^{27–29}, highlighting the need for novel OXA-48 inhibitors. Most β -lactamase inhibitors are directed towards class A β -lactamases but OXA enzymes share low sequence homology with class A³⁰. No OXA β -lactamase specific inhibitors have been clinically approved, but the β -lactam-based penicillin sulfones^{31,32} and non- β -lactams (phosphates/phosphonates, diazabicyclooctanes, and boronic acid-based compounds) have shown promise as inhibitors of OXA enzymes^{33,34}. Although the scaffolds of non- β -lactam-based inhibitors are unique, they are still ‘mechanism-based’ and similar to β -lactams in how they covalently inactivate β -lactamases. The ability of the KPC-2 β -lactamase to hydrolyze avibactam suggests variants can occur to inactivate non- β -lactam-based inhibitors²¹.

Although clinically available β -lactamase inhibitors utilize a covalent inactivation mechanism, non-covalent inhibitors may also be clinically viable. Promising non-mechanism-based OXA-48 inhibitors have been identified using fragment-based approaches^{35,36}. An orthogonal fragment screen using both SPR and inhibition assays was used to find new scaffolds and aided the development of an OXA-48 inhibitor with micromolar potency³⁵. This inhibitor was developed by merging the alternate conformations of a weaker pyridylbenzoic acid inhibitor seen in a co-crystal structure with OXA-48. This fragment study was continued with a focused library of monosubstituted benzoic acid fragments to further examine the OXA-48 binding pocket³⁶. Nevertheless, more potent inhibitors of OXA-48 inhibition are needed

DNA-encoded chemical libraries (DECLs) are combinatorial chemical libraries in which each compound is attached to a unique DNA molecule^{37–39}. The DNA molecule serves as a barcode, in which the different chemical building blocks are encoded by short, unique DNA sequences. This allows all the compounds to be pooled and screened against a target and subsequently, binding hits can be identified by sequencing the DNA tags using next-generation sequencing. DELs are typically synthesized with a split and pool approach to create combinatorial libraries with up to millions of compounds to efficiently scan chemical space^{39–42}. DNA-encoded chemistry technology has been used to identify inhibitors for various targets including the essential InhA enzyme in *Mycobacterium tuberculosis*⁴³, suggesting it could be expanded to other bacterial enzymes.

In this study, we describe the identification of two non- β -lactam OXA-48 inhibitors with sub-micromolar potency by using a DECL screening approach. Additionally, the X-ray crystal structure of one inhibitor in complex with OXA-48 was determined, and though *in vivo* potential is currently limited due to low accumulation in bacteria, this property can potentially be improved. DECLs have been used to identify inhibitors for a variety of proteins such as kinases, phosphatases, among others^{39,44,45}. To date, however, no β -

lactamase inhibitors have been reported using the DECL approach. This work suggests DECLs can provide new chemotypes for β -lactamase inhibition and may be a useful means to rapidly study the inhibition of β -lactamases and aid in the design of new inhibitors.

Results

DNA-encoded library synthesis and screening against OXA-48

A split and pool approach was used to create a combinatorial triazine-based library (Figure 1). Library members contained a double-stranded DNA portion, which functioned as the encoding DNA tag³⁹.

To build the triazine library, an initial array of building blocks (B1s) were linked to a short unique oligonucleotide sequence, coded to represent the specific building block added. All the unique DNA-linked compounds were pooled and attached to a triazine scaffold. This pool, containing the B1 building blocks attached to the triazine scaffold, was split and the set of B2 building blocks was added. A short oligonucleotide encoding the specific B2 building block was also ligated to the primary oligonucleotide. The compounds and associated DNA were then pooled again, split, and B3 building blocks were added and encoding oligonucleotides were ligated to the primary oligonucleotide to create a unique tag that encodes all attached building blocks for a given compound. After ligation, the compounds were pooled to form the final library, which contained approximately 162 million unique compounds. Details of library synthesis can be found in Supporting Information (Figures S1–S3).

For the selection of compounds that bind OXA-48, His-tagged OXA-48 was immobilized onto Ni-NTA agarose beads and incubated with the triazine library. A non-target control (NTC) with no enzyme that contained only the Ni magnetic beads was also screened against the library. After incubation, the beads were isolated and washed and the bound ligands were eluted. Two subsequent rounds of selection were performed with fresh immobilized OXA-48 to enrich for specific binders. The DNA tags of the recovered DECL compounds were amplified using PCR and NGS sequencing was performed to delineate the tag sequences. The identities of enriched compounds were determined by decoding DNA barcodes from the sequencing data set and translating them into their associated molecular components. Subsequently, the enrichment of each observed chemical species was evaluated. In our enrichment analysis strategy, a specific combination of building blocks is called an *n-synthon*, where *n* denotes the number of building blocks in the combination⁴⁶. Since the triazine library has three cycles of combinatorial synthesis, it contains *mono-*, *di-*, and *tri-synthons*. The enrichment of each observed *n-synthon* was analyzed by comparing its observed population to its expected population from a reference distribution⁴⁴. *N-synthon* classification is advantageous for both statistical and chemical analysis. Features with fewer synthons are expected to appear in the sampled data more frequently and thus are typically well-sampled. Such classification also allows rapid insight into structure-activity relationships and can suggest minimum pharmacophores necessary to yield enrichment in the affinity selection. OXA-48 hits were assessed by comparing the enrichment of *n-synthons* from the OXA-48 selection versus their corresponding enrichment in the non-target control selection. Enrichment was quantified using normalized z-scores⁴⁷ and depicted by

plotting the NTC z-score against the OXA-48 z-scores (Figure 2). Such screening provided a rapid means of identifying compounds enriched for binding to OXA-48. Enriched *n-synthons* from the library were used to guide the design and synthesis of compounds without DNA tags for biochemical evaluation.

Biochemical evaluation of synthon-derived compounds and lead identification

Compounds that were identified from DECL screening were re-synthesized without DNA tags. The activity of these compounds was assessed by *in vitro* inhibition assays with purified OXA-48. Compounds were tested for their ability to inhibit OXA-48 mediated hydrolysis of nitrocefin, a chromogenic β -lactam substrate routinely used in β -lactamase inhibition assays. Nitrocefin contains a conjugated ring system and produces a visible color shift from yellow to red upon hydrolysis⁴⁸. The rate of nitrocefin hydrolysis in the presence of a constant amount of OXA-48 and increasing concentrations of compound was plotted against compound concentration to determine the inhibition constant (K_i) towards OXA-48.

The most enriched *n-synthon* in the screen was a single *tri-synthon* compound with an enrichment score of 16 (Figure 2). These building blocks were assembled on to a triazine scaffold to create Compound 1 (Cmpd 1) (Figure 3). Cmpd 1 was enriched ~ 2-fold more than other highly enriched compounds that shared identical or similar building blocks at positions 2 and 3 (Figure 2). This suggested that either the unique building block at position 1 led to the increased enrichment of Cmpd 1 compared to similar *tri-synthons* or, alternatively, its enrichment was due to other reasons such as higher synthetic yield during library synthesis. Cmpd 1 showed near micromolar activity against purified OXA-48 ($K_i = 0.9 \pm 0.1 \mu\text{M}$) (Figure 3). Another interesting finding was that the *di-synthon* incorporating the building blocks from cycles 2 and 3 from Cmpd 1 was the fourth most enriched feature with a normalized enrichment of 7.2. Based on this finding, a series of compounds were synthesized using only building blocks in these positions on the triazine scaffold. These all contained the ethoxyphenyl-piperazine group, which was found in several highly enriched *di-* and *tri-synthons*. To rule out the possibility that the synthon at position 1 of Cmpd 1 (the fluoro-N-methylazetidide-3-carboxamide group) contributes to binding, Cmpds 2 and 3 were synthesized. Cmpd 3 contained the original B1 building block of Cmpd 1 with the ethoxyphenyl-piperazine while Cmpd 2 was similar but with a carboxylated B1 building block. (Figure 3). The OXA-48 active site, like that of all β -lactamases, contains a carboxylate binding pocket. For OXA-48, this pocket consists of residues Ser118, Thr209 and Arg250. Assuming the compounds bind the active site, it was predicted that the carboxamide group would be near this pocket. Therefore, Cmpd 2, a carboxylate derivative of Cmpd 3, was also synthesized. Both compounds showed minimal activity with K_i values $> 50 \mu\text{M}$ (Figure 3). These results suggest that the fluoro-N-methylazetidide-3-carboxamide group of Cmpd 1 does not contribute to inhibition. Next, the original highly enriched *di-synthon* was used to design Cmpd 4 (Figure 3). Cmpd 4 was the most potent of these derivatives with a K_i of $0.53 \pm 0.08 \mu\text{M}$ against OXA-48. This compound contained a carboxylate group that could potentially bind the carboxylate binding pocket of OXA-48. To test this hypothesis, Cmpd 5, which is an alkylated form of Cmpd 4, was also evaluated. Cmpd 5 exhibited a loss of activity ($K_i > 50 \mu\text{M}$), showing that the carboxylate in showing that the carboxylate in CDD-97 is indeed important for potency, consistent with an

interaction with the carboxylate binding pocket. Cmpd 4 showed the most promise against OXA-48 and was further investigated as the lead compound (CDD-97). Details of chemical synthesis can be found in Supporting Information.

Crystallization of CDD-97 with OXA-48

The structure of CDD-97 in complex with OXA-48 was determined to assess the binding site and facilitate medicinal chemistry modifications to enhance potency. The structure was determined by soaking OXA-48 apo crystals with CDD-97. The structure was solved in the $P6_5$ space group with 4 molecules in the asymmetric unit, each bound to a molecule of CDD-97, with occupancies of 85, 87, 88, and 89% (Table S1). The structure shows that CDD-97 binds in the active site of OXA-48 and makes several interactions, consistent with its relatively high potency (Figure 4). A polder mFo-Fc OMIT map confirmed the presence of the CDD-97 in the OXA-48 structure (Figure S5). The orientation of CDD-97 in the active site of all 4 monomers was identical, with small variations seen in the position of the rotatable carboxylate group, which was oriented to hydrogen bond with either 2 or 3 active site residues. The carboxylate of CDD-97 was confirmed to lie in the carboxylate binding pocket of OXA-48. This carboxylate group hydrogen bonds with Ser118, Thr209, and a salt bridge with Arg250, although its rotation leads to loss of the Ser118 interaction in some chains in the asymmetric unit. OXA-48, like all β -lactamases of its class, possesses a largely hydrophobic active site⁴⁹. The structure of the complex reveals that CDD-97 makes several hydrophobic interactions with OXA-48 including the triazine ring interacting with Ile102 and Tyr211, the piperazine ring interacting with Trp105, Leu158, and Thr213, and the terminal 2-ethoxyphenyl group interacting with Trp105, Val120, Leu158 (Figure 4). A comparison of the CDD-97/OXA-48 structure with the previously solved apo OXA-48 structure (PDB: 3HBR), the overall RMSD value of 0.39Å, which suggests there is not a significant change in overall residue positions between the two structures. In the apo OXA-48 structure, Arg214 forms hydrogen bonds with Asp159 and several water molecules, one of which additionally binds Gln124. In the CDD-97/OXA-48 complex, the inhibitor fills the active site and ultimately displaces Arg214, which is found at the base of the active site. Due to this movement, the electron density for the side chain of Arg214 is relatively weak, however it is clear that the stabilizing interactions that typically hold Arg214 in place in the apo structure are lost in the structure of the complex due to CDD-97 binding (Figure S6).

Structure-activity relationship studies

Several small-molecule derivatives of CDD-97 were created based on the inhibition and X-ray data to better understand the necessity of the different chemical moieties and gain insight for increasing potency (synthesis details are provided in Supporting Information). Derivatives were categorized by which ring was modified on CDD-97 (Figure 5) and are shown alongside their K_i values in Table 1. Structures of selected compounds in complex with OXA-48 were predicted by docking to gain insight into the molecular basis of changes in potency (Figure 6). The removal of ring 1 (ethoxyphenyl group), to create Cmpd 6, resulted in significant loss of potency ($K_i > 50 \mu\text{M}$). Docking results show the carboxylate group from the 4-carboxypiperidine ring retains strong interactions with Ser118, Lys208, Thr209, and Arg250 residues of the carboxylate binding pocket, suggesting the lack of the hydrophobic interactions resulting from the removal of the terminal 2-ethoxyphenyl ring

adversely affects binding (Figure 6). Other derivatives with modifications of this ring, Cmpds 7, 8 and 9, showed little change in potency (K_i values of 0.76, 1.7 and 2.2 μM respectively) compared to CDD-97 despite the addition of electronegative atoms. These results suggest ring 1 can tolerate additional substituents in its ortho-position and still maintain sufficient hydrophobic interactions to retain potency.

The piperazine ring (ring 2) also makes important hydrophobic interactions (Figures 4,5). Cmpds 10 and 11 were synthesized to test the effect of a linear chain replacing the piperazine ring. The introduction of flexibility from the linear chains at this position resulted in approximately a 16 to 40-fold reduction in potency for these derivatives, suggesting the shape and rigidity of the piperazine contributes to the inhibition potency. Docking results support this conclusion in that the carboxylate group from the 4-carboxypiperidine ring in Cmpd 10 retains strong interactions with Ser118, Lys208, Thr209, and Arg250 (Figure 6). However, the lack of the rigid piperazine ring gives rise to a more mobile terminal part of the ligand and with this atomic clash between the ligand and the binding pocket are possible. The triazine core (ring 3) makes hydrophobic interactions with Ile102 and pi-pi stacking interactions with the similarly aromatic Tyr211 residue (Figure 4). The addition of an amine group at the 6-position of the ring (Cmpd 13) does not have a large effect on potency even if followed by a longer ethylamine chain (Cmpd 12). Docking of Cmpd 12 shows the amine group is oriented towards the solvent and does not clash with residues in OXA-48 (Figure 6). This is consistent with the structures of the CDD97/OXA-48 complexes, which reveal this position is exposed to solvent (Figure 4). It is also consistent with the DECL selection data, as the triazine library had cycle 1 building blocks and the DNA linker in this position (Figures 1,2).

Finally, the 4-carboxypiperidine group (ring 4) showed the highest sensitivity to chemical modification (Table 1). This ring is situated above the Ser70 catalytic nucleophile in the OXA-48/CDD-97 structure, although it is not in direct contact with Ser70 (Figure 4). The carboxylate group of CDD-97 makes several hydrogen bonds to OXA-48 residues, which likely contributes to its potency. Substitution of the carboxylate group with an ester (Cmpd 5) (Figure 3) or a primary amide (Cmpd 14) resulted in a significant loss of inhibitory activity, as expected due to the loss of charge and hydrogen bonding potential (Table 1). It was not possible to obtain viable poses of Cmpd 5 by docking due to steric clashes while Cmpd 14 loses interactions with Ser118, Lys208, and Thr209 in the carboxylate binding pocket (Figure 6). Since the carboxypiperidine ring is close to Ser70, Cmpd 15 was designed with a primary amine added at position 4 to examine if the amine could interact with Ser70 or the carboxylated Lys73, which serves as the general base in OXA-48 catalysis. This resulted in a significant decrease in potency, suggesting the added amine may perturb the hydrogen bonding contribution of the carboxylate group. Docking results suggest that the added amino group clashes with the Ser118 side chain (Figure 6). The amino group also decreases the electron density of the carboxylate to weaken the hydrogen bonding and the salt bridge interactions with the residues in the carboxylate binding pocket.

Of all the derivatives, Cmpd 16, which substitutes the hydrogen bonding carboxylate group with sulfonic acid, showed an increase in potency ($K_i = 0.27 \pm 0.02 \mu\text{M}$). This two-fold increase in potency may be due to enhanced interactions of the sulfonic acid with the

carboxylate binding pocket. Consistent with this idea, docking results show salt bridges between the sulfonic acid and residues Lys208 and Arg250, as well as hydrogen bonds to Ser118, Thr209, and Arg250 (Figure 6).

Spectrum of activity with other OXA enzymes

The high sequence diversity of class D β -lactamases has made it difficult to identify a class-wide inhibitor^{10,50}. We tested the inhibition activity of CDD-97 against other OXA enzymes of varying sequence identity to assess its spectrum of activity (Table 2). OXA-10 is regarded as the canonical OXA enzyme, however, it is not a major clinical threat as it mainly hydrolyzes penicillins^{30,51,52}. OXA-24 and OXA-58 are also carbapenemases and, similar to OXA-48, they have poor activity against extended-spectrum cephalosporins^{53–55}. Unlike OXA-48, the OXA-24 and OXA-58 enzymes have a hydrophobic bridge in their active sites, which contributes to a preference for carbapenems with bulkier, more hydrophobic tails^{56,57}. OXA-48 is prevalent in *Enterobacteriaceae* (mainly *Klebsiella pneumoniae*) while OXA-24 and OXA-58 are prevalent in the *Moraxellaceae* family (mainly *Acinetobacter baumannii*)^{54,58}. While *K. pneumoniae* is more widespread in the clinics and most OXA-mediated carbapenem resistance is due to OXA-48, *A. baumannii* nosocomial infections are a growing problem. OXA-163 is an OXA-48-like enzyme also prevalent in *Enterobacteriaceae*⁵⁹. OXA-163 only differs from OXA-48 by a 4 amino acid deletion (Arg214 – Pro217), which gives it reduced carbapenemase activity but increased activity against extended-spectrum cephalosporins^{60,61}. OXA-163, as expected based on the high similarity to OXA-48, was inhibited by CDD-97 with a similar K_i as observed with OXA-48. OXA-10 and OXA-58 have lower sequence identities to OXA-48 (49.4% and 36.2% respectively) and were inhibited by CDD-97 with K_i values about 100-fold less potent than observed for OXA-48. CDD-97 displayed only a 26-fold decrease in potency for OXA-24 compared to OXA-48. Similar to OXA-58, OXA-24 has low sequence identity to OXA-48 (36.1%) and a hydrophobic bridge in the active site and yet is inhibited more potently by CDD-97 compared to OXA-58. Both enzymes contain a 2-residue hydrophobic bridge found to act as an inducible substrate binding cleft^{55,62}. However, OXA-58 additionally has a phenylalanine residue at the base of the active site which may further occlude the active site and perturb CDD-97 binding. Ultimately, CDD-97 inhibits other OXA enzymes but is much more potent towards OXA-48 and OXA-48-like enzymes.

Bacterial susceptibility and efficacy in *E. coli*

Clinically effective β -lactamase inhibitors synergize with β -lactam antibiotics and ultimately lower the minimum inhibitory concentration (MIC) of antibiotic needed to kill the bacteria⁶³. MIC studies of *E. coli* expressing the OXA-48 enzyme were performed with the β -lactam antibiotics ampicillin and imipenem (separately). Both of these antibiotics can be hydrolyzed by OXA-48⁶⁴. The OXA-48 plasmid construct contained the endogenous signal sequence of OXA-48 for secretion to the periplasm and was expressed under the control of the *trc*-promoter, which exhibits leaky expression in the absence of IPTG inducer⁶⁵. The construct was transformed into *E. coli* strain MG1655 for OXA-48 expression (MG1655_{OXA-48}). All MICs were performed by broth microdilution with 2-fold dilutions of antibiotic and/or inhibitor. The ampicillin (AMP) and imipenem (IMP) MICs were separately determined for a range of CDD-97 and avibactam concentrations. Avibactam was

used as a positive control since it has been shown to lower the MIC of β -lactams for bacteria expressing OXA-48²⁰. With increasing avibactam concentrations (up to 4 μ g/ml), there was a dose-dependent decrease in both the AMP and IMP MICs (Table 3). This confirmed that avibactam synergizes with β -lactam antibiotics to kill *E. coli* expressing OXA-48 and suggested that comparable inhibitors should exhibit a similar effect. The AMP MIC of *E. coli* MG1655_{OXA-48} in the absence of inhibitor was determined to be 512 μ g/ml. CDD-97 was then tested for synergy by determining AMP MICs with a range of CDD-97 concentrations. Higher concentrations of CDD-97 were used (up to 256 μ g/ml) due to its reduced potency against OXA-48 compared to avibactam²¹. At 256 μ g/ml of CDD-97, which corresponds to 0.6 mM and is over 1000-fold above the K_i for OXA-48, there was no significant decrease in the AMP MIC indicating CDD-97 did not synergize with ampicillin to enhance bacterial killing. Similarly, no synergy was seen between CDD-97 and imipenem in that the IMP MIC of 0.625 μ g/ml for *E. coli* MG1655_{OXA-48} did not decrease even at up to 256 μ g/ml of CDD-97 (Table 3). The poor activity of CDD-97 in the MIC assays compared to avibactam could be due to lower OXA-48 potency compared to avibactam²¹ and/or insufficient accumulation into the bacteria.

Impermeability of the outer membrane to small molecules is a major challenge for the development of therapeutics for Gram-negative bacterial infections⁶⁶⁻⁷⁰. β -lactamases, including OXA-48, reside in the periplasmic space and so inhibitors must traverse the outer membrane to be effective. To determine whether low permeability caused the poor *in vivo* activity of CDD-97, an accumulation assay was performed to quantify the amount of CDD-97 present in *E. coli* cells after incubation⁷¹. Tetracycline was used as a positive control for the assay while fusidic acid and clindamycin were used as negative controls⁷¹. The antibiotic controls and CDD-97 were separately incubated with wild-type *E. coli* cells and the cells were then centrifuged through silicone oil to separate the free, unaccumulated compounds from the cell pellet. Cell lysates were collected from the pellets by freeze-thawing and analyzed by mass spectrometry to quantify the amount of accumulated compound. CDD-97 was present in cells at 20-fold lower levels than the positive control tetracycline (Figure 7). These results indicate CDD-97 accumulates poorly in *E. coli*, explaining the lack of synergy with AMP and IMP in the MIC assay. The low accumulation of CDD-97 may be due to poor porin permeability to traverse the outer membrane and/or the action of efflux pumps that drive the compound out of the cell.

Discussion

β -lactamase inhibitors have been pivotal in managing antibiotic resistance mediated by β -lactamases. Most β -lactamase inhibitors are focused on class A β -lactamases. Initially, class D β -lactamases were of little clinical relevance but the emergence of carbapenemases such as OXA-48 has highlighted the need for OXA specific inhibitors due to their low sequence homology with class A enzymes³⁰. No OXA specific inhibitors have been clinically approved, but many have been developed and provide insight on OXA enzyme inhibition. The β -lactam based penicillin sulfones have efficacy against various OXA enzymes³¹. Specifically, the LN-1-255 inhibitor of this class is a 1000-fold more potent inhibitor of OXA-48 than is tazobactam and it increases the carbapenem susceptibility to bacteria expressing OXA-48³². Studies of phosphates/phosphonates, diazabicyclooctanes, and

boronic acid-based compounds have shown promise as inhibitors of OXA enzymes^{33,34}. However, since they maintain the typical acylation mechanism for β -lactamase inhibition, they may be susceptible to future variants that lead to rapid deacylation thereby reducing inhibitor potency.

To find more potent OXA-48 inhibitors, we utilized a DNA-encoded chemistry technology (DECL) approach. DECLs allow chemical space to be sampled more efficiently than typical high-throughput screening approaches. Additionally, tagging compounds with DNA allows rapid screening for faster identification of hits⁷². DECLs have helped identify hits for various targets such as kinases but there have been no reports of applications to β -lactamases^{45,72}. We utilized a DECL approach to identify OXA-48 inhibitors and gain insight into binding and inhibition.

Harnessing the efficiency of DECLs allowed for the identification of two sub-micromolar OXA-48 inhibitors, CDD-97 and its derivative Cmpd 16. CDD-97 was identified out of a library of ~160 million compounds, showing the potential of DNA-encoded chemistry technology. CDD-97 was one of the most enriched compounds in the screen and exhibited sub-micromolar inhibition potency. The insights gained from structure-activity relationship studies and the crystal structure of CDD-97 bound to OXA-48 were used to create a more potent inhibitor (Cmpd 16). This study provides more information regarding features that may be important for inhibition of OXA-48 and OXA-48 like enzymes in general, which can be expanded upon to find clinically useful inhibitors. Like previous inhibitors, we see the importance of an acidic group in the carboxylate binding pocket of OXA-48 as observed with CDD-97 and Cmpd 16. The inhibitors also revealed how the hydrophobic active site of OXA-48 can be utilized to impact potency. The inclusion of hydrophobic moieties to interact with hydrophobic residues comprising and surrounding the OXA-48 active site enhances potency.

Despite the poor efficacy *in vivo*, the discovery of sub-micromolar inhibitors is an advance towards designing clinically useful OXA-48 inhibitors since it has previously been difficult to identify potent inhibitors. Permeability is an important limiting factor for the discovery of antibacterial agents for Gram-negative bacteria. The selective permeability of the outer membrane and porins limit access of compounds into the cell. Uptake of antimicrobials is further complicated by efflux pumps, which typically have a broad spectrum of activity⁶⁸. Hydrophobic compounds are more susceptible to efflux pumps, which trap compounds through hydrophobic and stacking interactions⁷³. CDD-97 is largely hydrophobic and potentially susceptible to efflux pumps but may also have low porin permeability ultimately leading to its poor accumulation. The poor activity of CDD-97 and ampicillin against *E. coli* expressing OXA-48 due to low access to the periplasm was corroborated by mass spectrometry studies revealing it accumulated poorly into *E. coli* (Figure 7). Accumulation studies have shown that compounds exhibit enhanced entry into bacteria if they are rigid, amphiphilic, flat and contain a primary amine⁷¹. Primary amines that are not sterically hindered were found to aid accumulation and even broaden the spectrum of activity of compounds to include Gram-positive bacteria⁷¹. However, the addition of amines is insufficient for increasing accumulation if the flexibility and globularity of the compound are too high. Calculations from the *Entryway*⁷¹ server (which provides predictions for

accumulation in Gram-negative bacteria) revealed that while CDD-97 has reasonable globularity it is not sufficiently rigid. Globularity was computationally ranked on a scale from 0 – 1 with 0 representing flatness (i.e. benzene) and 1 representing sphericity (i.e. adamantane). CDD-97 yielded a globularity score of 0.061 falling within the range of low globularity (globularity < 0.25) as previously described⁷¹. Accumulation studies also revealed low flexibility (having 5 or fewer rotatable bonds) was also important for accumulation and CDD-97 was found to have 6 rotatable bonds, potentially explaining its poor accumulation when the lack of primary amines is also considered. The accumulation of CDD-97 could potentially be optimized by decreasing its flexibility and by the strategic addition of 1 or more primary amines. Such modifications are predicted based on steered molecular dynamics to aid with traversing porins, particularly the major OmpF porin, which, along with OmpC, is responsible for a significant amount of drug accumulation⁷¹. A primary amine on a rigid compound is predicted to be more available and accessible and thus able to interact with the key Asp113 residue of OmpF, which can modulate the porin's constriction site to assist passage⁷¹. Although CDD-97 may also be susceptible to efflux pumps, modifications for more efficient porin passage could potentially allow the compound to accumulate sufficiently to inhibit OXA-48 in the periplasm before being removed by efflux pumps on the cytoplasmic membrane. While many effective antibacterial agents deviate from the predicted accumulation trends, these parameters allow notable prediction of accumulation⁷¹ and show promise to aid in optimizing compounds to enter bacteria. This could be particularly powerful for potent β -lactamase inhibitors that may accumulate poorly. With the increasing number of problematic β -lactamases, expediting the identification of potent, high-accumulating inhibitors will be vital to manage resistance.

Conclusion

This work highlights DEL-based drug discovery with DNA-encoded chemistry technology as an effective approach that could be applied to various β -lactamases to study their inhibition and potentially design useful inhibitors. The power of such libraries could be amplified in the future by creating focused libraries specifically tailored to β -lactamases, particularly OXA-48 and other carbapenemases. Despite the high sequence variability between classes of serine β -lactamases, they all contain a carboxylate binding pocket that favors negatively charged moieties. This could prove to be an effective strategy to rapidly find lead compounds to aid in developing β -lactamase inhibitors. Additionally, DEL screening can be modular and include rounds of screening with different targets or allow screening of multiple targets in parallel. This could potentially be used to remove binders to a given β -lactamase from the pool of compounds to find specific binders for another β -lactamase or to uncover a broad-spectrum inhibitor with efficacy across β -lactamase classes. There is great potential for the application of DNA-encoded chemistry technology to β -lactamase inhibitor drug discovery. The speed at which leads can be found will be a useful tool to study β -lactamase inhibition to ultimately aid inhibitor design to manage growing β -lactamase-mediated resistance.

Experimental Section

Protein expression and purification

His-tagged OXA-48 was expressed from a pET28a vector under the IPTG inducible T7 promoter in *E. coli* BL21(DE3) cells^{74–76}. In the pET28a vector, the thrombin site used to cleave the N-terminal His-tag was changed to a TEV cleavage site. Cultures were grown to an OD₆₀₀ of 0.4 – 0.8 in media containing 25 µg/mL kanamycin, then induced for protein expression by adding IPTG to a final concentration of 0.5 mM and incubating for 18 – 20 hours at 25°C. The cell pellets were collected by centrifugation and frozen at –20°C. For cell lysis, frozen pellets were resuspended in 50 mM HEPES pH 7.5, 0.05% octyl-β-D-glucopyranoside buffer and sonicated with pauses to avoid sample heating. Cell lysates were filtered using 0.45 µm filters and then loaded onto a His Trap HP column (GE Healthcare, Pittsburg, PA). His-tagged OXA-48 was eluted using a linear gradient with 500 mM imidazole in 50 mM HEPES pH 7.5 buffer. NaCl was excluded from the buffer because a high concentration of chloride ions can inhibit OXA-48. Fractions were checked on SDS-PAGE gels and fractions with contaminants were excluded before concentrating using Amicon centrifugal filters with a 10,000 MW cut-off (Merck KGaA, Darmstadt, Germany). After concentrating, the protein was further purified by size-exclusion chromatography using a HiLoad 10/300 Superdex 75 column (GE Healthcare) in 50 mM HEPES pH 7.5, 15 mM NaHCO₃. Fractions were examined by SDS-PAGE before concentrating and cleaving off the N-term His-tag using TEV protease. The His-tagged version of OXA-48 without cleaving the tag was used for compound screening and SPR assays. Inhibition assays and X-ray crystallography experiments were performed using OXA-48 with the tag removed.

Synthesis of DNA-free compounds and derivatives for inhibition assays

All compounds were procured through Sigma-Aldrich and Fisher Scientific. NMR spectra were collected using a Bruker 600 MHz NMR. LCMS data was collected using an Agilent 1290 Infinity Series LC system with 6150 MS. Column used was Agilent Eclipse Plus C18, 2.1 mm x 50 mm (8 µm). Mobile phase solvents were A: 0.05% formic acid; B: 5% water in acetonitrile. Runs consisted of 5% A for 0.5 minutes, gradient over 3 minutes of 5% A to 95% A, then 95% A over 1 minute. Synthesis of individual derivatives can be found in the Supporting Information.

Affinity selection with DNA-encoded chemistry technology

DNA-encoded chemical libraries were incubated with 1µM of His-OXA-48 in 200 µL of selection buffer (20 mM HEPES, 134 mM KOAc, 8 mM NaOAc, 4 mM NaCl, 0.8 mM MgOAc, 5 mM imidazole, 0.02% Tween-20 (pH 7.2)) supplemented with 0.1mg/ml sheared salmon sperm DNA and 15 mM NaHCO₃ for 45 min at 25 °C on a thermomixer (1000 RPM). The same library pool without protein was also incubated under the same conditions as a negative control to assess background binding of DECL molecules to the affinity resin. Before incubation, 1 µL of library molecules were set aside for quantitation using quantitative PCR (qPCR). Ni-NTA magnetic beads (25µL) were prewashed with selection buffer and the target protein–library mixture was added for affinity selection. The magnetic beads were washed with 500 µL of selection buffer to remove unbound DECL molecules. Bound compounds were eluted by incubating the beads with 100 µL of selection buffer at 80

°C for 10 min. One microliter of elution material was again set aside for quantitation by qPCR, and the entire remaining volume of the sample was subjected to an additional two rounds of affinity selection with fresh protein as mentioned above. After 3 rounds of selection, DECL molecules were quantified by qPCR which serves as a quality control measure. qPCR is done on each sample of recovered DECL material after each round of selection to monitor the total amount of DNA tags remaining. This information is used to guide both the selection process and sequencing preparation.

An appropriate number of PCR cycles was used to amplify the DNA and add DNA sequences compatible with Illumina sequencing flow cells. The PCR product was purified using Agencourt AMPure XP SPRI beads (Agencourt, Danvers, MA) according to the manufacturer's instructions, and then quantitated on an Agilent BioAnalyzer (Santa Clara, CA) using a high-sensitivity DNA kit. The final concentration of amplicon for each sample was pooled at a concentration of between 3 and 4 nM. The final concentration of 1.8 pM library pool samples were loaded onto an Illumina Next-Seq 500 sequencer (San Diego, CA) at the Genomic and RNA Profiling Core Facility at Baylor College of Medicine.

Steady state kinetics with nitrocefin substrate

Nitrocefin, a chromogenic β -lactam substrate, was used as a reporter in all inhibition assays with the various OXA enzymes and various compounds. Nitrocefin is not stable in aqueous solution long-term. For these assays, nitrocefin stocks were prepared in DMSO, stored at -20°C and used within 2 weeks of dissolving. To avoid freeze-thawing, fresh stocks were always used. The K_m of nitrocefin was determined prior to inhibition assays by performing steady state kinetics. Assays were performed using a DU800 spectrophotometer at room temperature in 50 mM HEPES pH 7.5, 15 mM NaHCO_3 , and 0.02% tween-20. Hydrolyzed nitrocefin was detected at 482 nm. For a single experiment, a series of at least 5 nitrocefin concentrations were tested against the given enzyme in duplicate and the initial velocities were measured and fit to the Michaelis-Menten equation. Experiments were repeated twice, and error reported is the standard error of the mean.

$$V_0 = \frac{V_{\max}[S]}{(K_M + [S])}$$

Inhibition assays using nitrocefin as reporter

Compounds were tested for inhibition of a given OXA enzyme based on the hydrolysis of nitrocefin using a Tecan plate reader. A nitrocefin concentration near the K_m was used with a constant concentration of OXA-48 and a range of 6 concentrations of the compound of interest (10 μM with 3-fold serial dilutions) were tested in duplicate. A control with no compound was included in each run. For each compound concentration, the velocity of nitrocefin hydrolysis was determined at 482 nm and fit to the Morrison equation⁷⁷. Compounds that exhibited K_i values above 50 μM were simply denoted as having a K_i value $>50 \mu\text{M}$. The average K_i of separate experiments, each of which consisted of duplicate runs, is reported and error was quantified as the standard deviation.

Crystallography and data collection

Hanging drops were set up to obtain crystals via the vapor diffusion method either manually or using an automated Mosquito robot. Crystallization conditions were screened with commercially available screens from Hampton Research (Aliso Viejo, CA) and Qiagen (Venlo, Netherlands) using a 96-well format. Initial crystallization conditions were optimized by varying pH and precipitant concentrations. The CDD-97/OXA-48 structure was determined from an apo crystal that grew from a 1:1 (protein to reservoir solution) mixture of 7.1 mg/mL OXA-48 and 0.077 M Tris pH 8, 27% PEG 550 MME, which was later soaked with a 1 μ L drop of 2 mM CDD-97. For soaking, a 10 mM DMSO stock of CDD-97 was diluted 1:1 in 100% 2-Methyl-2,4-pentanediol, and then diluted in the crystal buffer for a final concentration of 2 mM. The data sets were collected at the Berkeley Center for Structural Biology in the context of the Collaborative Crystallography Program on beamline 5.0.2

Crystallography data processing and refinement

Diffraction data were processed using the HKL2000 software, molecular replacement (PHASER) and initial refining (REFMAC) were performed using the CCP4 suite^{78,79}. Molecular replacement was performed using the OXA-48 structure (PDB ID: 3HBR) as the search model. Further refinements were performed using the PHENIX software (phenix.refine)⁸⁰. The structure was manually examined throughout the structure completion process after molecular replacement, using the Crystallography Object-Oriented Toolkit (COOT) program⁸¹. When appropriate, TLS groups were determined using the TLSMD server. The final refinement was done using phenix.refine and the final structure was inspected and validated with MolProbity and COOT^{81,82}. The electron density of CDD-97 bound to OXA-48 in the crystal structure was further examined by creating a polder mFo-Fc OMIT map using the PHENIX software⁸⁰.

Docking Protocol for the CDD-97 Derivatives into OXA-48

The images show the derivatives of CDD-97 docked into OXA-48 obtained from the CDD-97/OXA-48 co-crystal structure. To collect these poses, first the protein from the crystal structure was processed by the Schrodinger Suite Release 2018-3⁸³: First, bond orders were assigned and H atoms were added by the Protein Preparation Wizard⁸⁴. Then, the hydrogen bonding networks were optimized according to the protonation states determined by the program PROPKA⁸⁵ at a neutral pH. Finally, the entire structure was energy-minimized where the heavy atoms were restrained to deviate from their original locations to a max. of 0.30 Å. A grid was generated at the site of the native crystal ligand for small molecule docking. The docked CDD-97 derivatives were prepared with the LigPrep program. This entails obtaining accurate 3D-structures of the ligands in their correctly assigned protonation states by the program Epik^{86,87}. The prepared ligands were docked into the aforementioned grid using the Glide⁸⁸⁻⁹⁰ program in the extra precision (XP) mode. The shown poses were extracted from the docking results and visualized by the Maestro⁹¹ program, which was also used to render the figures.

Bacterial susceptibility in *E. coli*

Bacterial susceptibility was specifically tested using minimum inhibitory concentration assays. Susceptibility assays were performed with *E. coli* strains using broth microdilution in a microtiter plate. Two-fold dilutions of antibiotic and/or inhibitor were used. For susceptibility tests, bacterial strains were transformed with plasmids containing OXA-48 with its endogenous signal sequence for periplasmic migration (cloned into the pTP470 vector)⁹². *E. coli* MG1655 bacteria were grown in Mueller-Hinton broth overnight with 12.5 µg/mL chloramphenicol to select for the OXA-48-containing pTP470 plasmid. An overnight culture was diluted 1:10⁴ into the final well solutions and incubated for 16-18 hours. After incubation, microplates were read using a Tecan plate reader at 600 nm absorbance. Growth was defined as yielding an absorbance 2 times the absorbance of the negative control (media and no culture).

Accumulation assays in *E. coli*

For the accumulation assay, the protocol from Ritcher et al.⁷¹ was followed. An overnight culture of *E. coli* MG1655 bacteria grown in LB Lennox broth, was inoculated into fresh media and grown to an OD₆₀₀ of 0.5 - 0.6. Cells were pelleted, resuspended in 1x phosphate-buffered saline (PBS) and then incubated with the compound of interest for 10 minutes at 37°C. After incubation, the OD₆₀₀ was recorded to note if compounds affected cell growth and then the cultures were centrifuged through a 9:1 mixture of silicone oil (viscosity = 20 cST) to high temperature silicone oil which was cooled at -80 °C. Cell pellets were isolated and lysed by 3 cycles of freeze-thawing using liquid nitrogen and a 65 °C water bath. The cell lysate was isolated from the cell debris (in water and methanol) and then analyzed via liquid chromatography-mass spectrometry (Agilent Technologies, 6490 QQQ Santa Clara, CA). LC-MS/MS was operated in positive mode for tetracycline, clindamycin, and CDD-97 and in negative mode for fusidic acid with electrospray ionization. Multiple reaction monitoring (MRM) was used to quantify these compounds. The precursors to production transitions of these compounds were as follows: m/z 445.16 > 153.70 (tetracycline); 425.14 > 126.10 (clindamycin); 515.30 > 455.20 (fusidic acid); 413.23 > 249.50 (CDD-97). The concentrations of these compounds were calculated based on their corresponding standard curves.

To determine the colony forming units (CFU) per mL based on the OD₆₀₀, the OD₆₀₀ of *E. coli* MG1655 culture in LB-Lennox was measured then the culture was diluted and plated to count colonies. Based on this, the CFU per mL for 1 O.D.₆₀₀ (for MG1655 cells grown in LB-Lennox) was determined to be approximately 2.15 x 10⁸ and this value was used for accumulation calculations.

Supplementary Material

Refer to Web version on PubMed Central for supplementary material.

Acknowledgements

The authors thank Dr. Ying-Chu Chen from the Center for Drug Discovery at Baylor College of Medicine (Houston, TX) for providing Figure S4.

Funding

This work was supported by NIH grants AI143832 and AI32956 (to TP) and T32 GM120011 (to DT). This research used resources of the Advanced Light Source, which is a DOE Office of Science User Facility under contract no. DE-AC02-05CH11231. The ALS-ENABLE beamlines are supported in part by the National Institutes of Health, National Institute of General Medical Sciences, grant P30 GM124169-01. DNA-encoded chemical library production in the Center for Drug Discovery work is supported by a Core Facility Support Award from the Cancer Prevention Research Institute of Texas (RP160805), and the Welch Foundation (Grant H-Q-0042).

References

- (1). U.S. Department of Health and Human Services, C. for D. C. and P. Antibiotic Resistance Threats in the United States, 2013. *Current* 2013, 114 <https://doi.org/CS239559-B>.
- (2). Bush K; Bradford PA β -Lactams and β -Lactamase Inhibitors: An Overview. *Cold Spring Harb. Perspect. Med.* 2016, 6 (8), a025247 10.1101/cshperspect.a025247. [PubMed: 27329032]
- (3). Poole K Resistance to β -Lactam Antibiotics. *Cell. Mol. Life Sci.* 2004, 61 (17), 2200–2223. 10.1007/s00018-004-4060-9. [PubMed: 15338052]
- (4). Elander RP Industrial Production of β -Lactam Antibiotics. *Appl. Microbiol. Biotechnol.* 2003, 61 (5–6), 385–392. 10.1007/s00253-003-1274-y. [PubMed: 12679848]
- (5). Blumer KJ; Thorner J Cutting and Stitching: The Cross-Linking of Peptidoglycan in the Assembly of the Bacterial Cell Wall. *ACS Chem. Biol.* 2007, 2 (12), 783–786. [PubMed: 18154265]
- (6). Kitano K; Tomasz A Triggering of Autolytic Cell Wall Degradation in *Escherichia Coli* by Beta-Lactam Antibiotics. *Antimicrob. Agents Chemother.* 1979, 16 (6), 838–848. 10.1128/AAC.16.6.838. [PubMed: 93877]
- (7). Abraham EP and Chain E An Enzyme from Bacteria Able to Destroy Penicillin. *Oxford Journals* 1988, 10 (4), 677–678.
- (8). Wright GD; Poinar H Antibiotic Resistance Is Ancient: Implications for Drug Discovery. *Trends Microbiol.* 2012, 20 (4), 157–159. 10.1016/j.tim.2012.01.002. [PubMed: 22284896]
- (9). Bush K Bench-to-Bedside Review: The Role of β -Lactamases in Antibiotic-Resistant Gram-Negative Infections. *Crit. Care* 2010, 14 (3). 10.1186/cc8892.
- (10). Drawz SM; Bonomo RA Three Decades of β -Lactamase Inhibitors. *Clin. Microbiol. Rev.* 2010, 23 (1), 160–201. 10.1128/CMR.00037-09. [PubMed: 20065329]
- (11). Naas T; Oueslati S; Bonnin RA; Dabos ML; Zavala A; Dortet L; Retailleau P; Iorga BI Beta-Lactamase Database (BLDB)–Structure and Function. *J. Enzyme Inhib. Med. Chem.* 2017, 32 (1), 917–919. 10.1080/14756366.2017.1344235. [PubMed: 28719998]
- (12). Guh AY; Limbago BM; Kallen AJ Epidemiology and Prevention of Carbapenem-Resistant Enterobacteriaceae in the United States. *Expert Rev. Anti. Infect. Ther.* 2014, 12 (5), 565–580. 10.1586/14787210.2014.902306. [PubMed: 24666262]
- (13). Logan LK; Weinstein RA The Epidemiology of Carbapenem-Resistant Enterobacteriaceae: The Impact and Evolution of a Global Menace. *J. Infect. Dis.* 2017, 215 (Suppl 1), S28–S36. 10.1093/infdis/jiw282. [PubMed: 28375512]
- (14). Papp-Wallace KM; Endimiani A; Taracila MA; Bonomo RA Carbapenems: Past, Present, and Future. *Antimicrob. Agents Chemother.* 2011, 55 (11), 4943–4960. 10.1128/aac.00296-11. [PubMed: 21859938]
- (15). Doi Yohei & Paterson, David L Carbapenemase-Producing Enterobacteriaceae. *Semin. Respir. Crit. Care Med.* 2016, 36 (1), 74–84. 10.1055/s-0035-1544208. Carbapenemase-Producing.
- (16). Nordmann P; Dortet L; Poirel L Carbapenem Resistance in Enterobacteriaceae: Here Is the Storm! *Trends Mol. Med.* 2012, 18 (5), 263–272. 10.1016/j.molmed.2012.03.003. [PubMed: 22480775]
- (17). Queenan AM; Bush K Carbapenemases: The Versatile β -Lactamases. *Clin. Microbiol. Rev.* 2007, 20 (3), 440–458. 10.1128/CMR.00001-07. [PubMed: 17630334]
- (18). Ambler RP The Structure of β -Lactamases. 1983, 331 (1969), 75–97.
- (19). Bush K; Jacoby GA Updated Functional Classification of β -Lactamases. *Antimicrob. Agents Chemother.* 2010, 54 (3), 969–976. 10.1128/AAC.01009-09. [PubMed: 19995920]

- (20). Akta Z; Kayacan C; Oncul O In Vitro Activity of Avibactam (NXL104) in Combination with β -Lactams against Gram-Negative Bacteria, Including OXA-48 β -Lactamase-Producing *Klebsiella Pneumoniae*. *Int. J. Antimicrob. Agents* 2012, 39 (1), 86–89. 10.1016/j.ijantimicag.2011.09.012. [PubMed: 22041508]
- (21). Ehmann DE; Jahi H; Ross PL; Gu RF; Hu J; Durand-Réville TF; Lahiri S; Thresher J; Livchak S; Gao N; Palmer T; Walkup GK; Fisher SL Kinetics of Avibactam Inhibition against Class A, C, and D β -Lactamases. *J. Biol. Chem.* 2013, 288 (39), 27960–27971. 10.1074/jbc.M113.485979. [PubMed: 23913691]
- (22). Gu R-F; Jahic H; Kern G; Ross PL; Ehmann DE; Hu J; Fisher SL; Walkup GK Avibactam Is a Covalent, Reversible, Non- β -Lactam β -Lactamase Inhibitor. *Proc. Natl. Acad. Sci.* 2012, 109 (29), 11663–11668. 10.1073/pnas.1205073109. [PubMed: 22753474]
- (23). Ripoll A; Galán JC; Rodríguez C; Tormo N; Gimeno C; Baquero F; Martínez-Martínez L; Cantón R Detection of Resistance to Beta-Lactamase Inhibitors in Strains with CTX-M Beta-Lactamases: A Multicenter External Proficiency Study Using a Well-Defined Collection of *Escherichia Coli* Strains. *J. Clin. Microbiol.* 2014, 52 (1), 122–129. 10.1128/JCM.02340-13. [PubMed: 24153133]
- (24). Stapleton P; Wu PJ; King A; Shannon K; French G; Phillips I Incidence and Mechanisms of Resistance to the Combination of Amoxicillin and Clavulanic Acid in *Escherichia Coli*. *Antimicrob. Agents Chemother.* 1995, 39 (11), 2478–2483. 10.1128/AAC.39.11.2478. [PubMed: 8585729]
- (25). Winkler ML; Papp-Wallace KM; Taracila MA; Bonomo RA Avibactam and Inhibitor-Resistant SHV β -Lactamases. *Antimicrob. Agents Chemother.* 2015, 59 (7), 3700–3709. 10.1128/aac.04405-14. [PubMed: 25691639]
- (26). Drawz SM; Papp-Wallace KM; Bonomo RA New β -Lactamase Inhibitors: A Therapeutic Renaissance in an MDR World. *Antimicrob. Agents Chemother.* 2014, 58 (4), 1835–1846. 10.1128/AAC.00826-13. [PubMed: 24379206]
- (27). Wu J; Racine F; Wismer MK; Young K; Carr DM; Xiao JC; Si Q; Katwaru R; Harradine P; Motyl M; Bhagunde PR; Rizk ML Exploring the Pharmacokinetic/Pharmacodynamic Relationship of Relebactam (MK-7655) in Combination with Imipenem in a Hollow-Fiber Infection Model. *Antimicrob. Agents Chemother.* 2018, 62 (5), 1–13. 10.1128/aac.02323-17.
- (28). van Duin D; Bethel CR; Kreiswirth BN; Becka SA; Bonomo RA; Taracila MA; Papp-Wallace KM; Barnes MD; Alsop J; Kaye KS Relebactam Is a Potent Inhibitor of the KPC-2 β -Lactamase and Restores Imipenem Susceptibility in KPC-Producing Enterobacteriaceae. *Antimicrob. Agents Chemother.* 2018, 62 (6), 1–9. 10.1128/aac.00174-18.
- (29). Lomovskaya O; Sun D; Rubio-Aparicio D; Nelson K; Tsivkovski R; Griffith DC; Dudley MN Vaborbactam: Spectrum of Beta-Lactamase Inhibition and Impact of Resistance Mechanisms on Activity in Enterobacteriaceae. *Antimicrob. Agents Chemother.* 2017, 61 (11), 1–15. 10.1128/AAC.01443-17.
- (30). Evans BA; Amyes SGB OXA β -Lactamases. *Clin. Microbiol. Rev.* 2014, 27 (2), 241–263. 10.1128/CMR.00117-13. [PubMed: 24696435]
- (31). Drawz SM; Bethel CR; Doppalapudi VR; Sheri A; Pagadala SRR; Hujer AM; Skalweit MJ; Anderson VE; Chen SG; Buynak JD; Bonomo RA Penicillin Sulfone Inhibitors of Class D β -Lactamases. *Antimicrob. Agents Chemother.* 2010, 54 (4), 1414–1424. 10.1128/AAC.00743-09. [PubMed: 20086146]
- (32). Martínez-Gutián M; Vallejo JA; Poza M; Vázquez-Ucha JC; Bou G; González-Bello C; Bonomo RA; Beceiro A; Bethel CR; Buynak JD LN-1-255, a Penicillanic Acid Sulfone Able to Inhibit the Class D Carbapenemase OXA-48. *J. Antimicrob. Chemother.* 2016, 71 (8), 2171–2180. 10.1093/jac/dkw105. [PubMed: 27125555]
- (33). Majumdar S; Adediran SA; Nukaga M; Pratt RF Inhibition of Class D β -Lactamases by Acyl Phosphates and Phosphonates. *Biochemistry.* 2005, 44 (49), 16121–16129. 10.1128/AAC.49.10.4410. [PubMed: 16331972]
- (34). Werner JP; Mitchell JM; Taracila MA; Bonomo RA; Powers RA Exploring the Potential of Boronic Acids as Inhibitors of OXA-24/40 β -Lactamase. *Protein Sci.* 2017, 26 (3), 515–526. 10.1002/pro.3100. [PubMed: 27997706]

- (35). Lund BA; Christopheit T; Guttormsen Y; Bayer A; Leiros HKS Screening and Design of Inhibitor Scaffolds for the Antibiotic Resistance Oxacillinase-48 (OXA-48) through Surface Plasmon Resonance Screening. *J. Med. Chem.* 2016, 59 (11), 5542–5554. 10.1021/acs.jmedchem.6b00660. [PubMed: 27165692]
- (36). Akhter S; Lund BA; Ismael A; Langer M; Isaksson J; Christopheit T; Leiros HKS; Bayer A A Focused Fragment Library Targeting the Antibiotic Resistance Enzyme - Oxacillinase-48: Synthesis, Structural Evaluation and Inhibitor Design. *Eur. J. Med. Chem.* 2018, 145, 634–648. 10.1016/j.ejmech.2017.12.085. [PubMed: 29348071]
- (37). Brenner S; Lerner RA Encoded Combinatorial Chemistry. *Proc. Natl. Acad. Sci.* 2006, 89 (12), 5381–5383. 10.1073/pnas.89.12.5381.
- (38). Melkko S; Dumelin CE; Scheuermann J; Neri D Lead Discovery by DNA-Encoded Chemical Libraries. *Drug Discov. Today* 2007, 12 (11–12), 465–471. 10.1016/j.drudis.2007.04.007. [PubMed: 17532531]
- (39). Clark MA; Acharya RA; Arico-Muendel CC; Belyanskaya SL; Benjamin DR; Carlson NR; Centrella PA; Chiu CH; Creaser SP; Cuzzo JW; Davie CP; Ding Y; Franklin GJ; Franzen KD; Gefter ML; Hale SP; Hansen NJV; ... Morgan BA Design, Synthesis and Selection of DNA-Encoded Small-Molecule Libraries. *Nat. Chem. Biol.* 2009, 5 (9), 647–654. 10.1038/nchembio.211 [PubMed: 19648931]
- (40). MacConnell AB; McEnaney PJ; Cavett VJ; Paegel BM DNA-Encoded Solid-Phase Synthesis: Encoding Language Design and Complex Oligomer Library Synthesis. *ACS Comb. Sci.* 2015, 17 (9), 518–534. 10.1021/acscmbosci.5b00106. [PubMed: 26290177]
- (41). Škopi MK; Bugain O; Jung K; Onstein S; Brandherm S; Kalliokoski T; Brunschweiler A Design and Synthesis of DNA-Encoded Libraries Based on a Benzodiazepine and a Pyrazolopyrimidine Scaffold. *Medchemcomm* 2016, 7 (10), 1957–1965. 10.1039/c6md00243a.
- (42). Yuen LH; Franzini RM Achievements, Challenges, and Opportunities in DNA-Encoded Library Research: An Academic Point of View. *ChemBioChem* 2017, 18 (9), 829–836. 10.1002/cbic.201600567. [PubMed: 28032411]
- (43). Soutter HH; Centrella P; Clark MA; Cuzzo JW; Dumelin CE; Guie M-A; Habeshian S; Keefe AD; Kennedy KM; Sigel EA; Troast DM; Zhang Y; Ferguson AD; Davies G; Stead ER; Breed J; Madhavapeddi P; Read JA Discovery of Cofactor-Specific, Bactericidal Mycobacterium Tuberculosis InhA Inhibitors Using DNA-Encoded Library Technology. *Proc. Natl. Acad. Sci.* 2016, 113 (49), E7880–E7889. 10.1073/pnas.1610978113. [PubMed: 27864515]
- (44). Barluenga S; Zambaldo C; Ioannidou HA; Ciobanu M; Morieux P; Daguier JP; Winssinger N Novel PTP1B Inhibitors Identified by DNA Display of Fragment Pairs. *Bioorganic Med. Chem. Lett.* 2016, 26 (3), 1080–1085. 10.1016/j.bmcl.2015.11.102.
- (45). Kleiner RE; Dumelin CE; Tiu GC; Sakurai K; Liu DR In Vitro Selection of a DNA-Templated Small-Molecule Library Reveals a Class of Macrocyclic Kinase Inhibitors. *J. Am. Chem. Soc.* 2010, 132 (33), 11779–11791. 10.1021/ja104903x. [PubMed: 20681606]
- (46). Faver JC; Riehle K; Lancia DR; Milbank JBJ; Christopher S Supporting Information for “ Quantitative Comparison of Enrichment from DNA-Encoded Chemical Library Selections ” Table of Contents. 1–31.
- (47). Faver JC; Riehle K; Yu Z; Kollmann CS; Milbank JBJ; Lancia DR; Simmons N; Matzuk MM Quantitative Comparison of Enrichment from DNA-Encoded Chemical Library Selections. *ACS Comb. Sci.* 2019, 1–28. 10.1021/acscmbosci.8b00116.
- (48). O’Callaghan CH; Morris A; Kirby SM; Shingler AH Novel Method for Detection of Beta-Lactamases by Using a Chromogenic Cephalosporin Substrate. *Antimicrob. Agents Chemother.* 1972, 1 (4), 283–288. 10.1128/AAC.1.4.283. [PubMed: 4208895]
- (49). Leonard DA; Bonomo RA; Powers RA Class D β -Lactamases: A Reappraisal after Five Decades. *Acc. Chem. Res.* 2013, 46 (11), 2407–2415. 10.1021/ar300327a. [PubMed: 23902256]
- (50). Poirel L; Naas T; Nordmann P Diversity, Epidemiology, and Genetics of Class D β -Lactamases. *Antimicrob. Agents Chemother.* 2010, 54 (1), 24–38. 10.1128/AAC.01512-08. [PubMed: 19721065]

- (51). Paetzel M; Danel F; De Castro L; Mosimann SC; Page MGP; Strynadka NCJ Crystal Structure of the Class D β -Lactamase OXA-10. *Nat. Struct. Biol.* 2000, 7 (10), 918–925. 10.1038/79688. [PubMed: 11017203]
- (52). Mobashery S; Samama J-P; Maveyraud L; Golemi D; Vakulenko S Critical Involvement of a Carbamylated Lysine in Catalytic Function of Class D β -Lactamases. *Proc. Natl. Acad. Sci.* 2002, 98 (25), 14280–14285. 10.1073/pnas.241442898.
- (53). Santillana E; Beceiro A; Bou G; Romero A Crystal Structure of the Carbapenemase OXA-24 Reveals Insights into the Mechanism of Carbapenem Hydrolysis. *Proc. Natl. Acad. Sci.* 2007, 104 (13), 5354–5359. 10.1073/pnas.0607557104. [PubMed: 17374723]
- (54). Poirel L; Marque S; He C; Segonds C; Nordmann P OXA-58, a Novel Class D β -Lactamase Involved in Resistance to Carbapenems in *Acinetobacter Baumannii*. *Society* 2005, 49 (1), 202–208. 10.1128/AAC.49.1.202.
- (55). Ishii Y; Ueno G; Miyano M; Saino H; Sugiyabu T; Yamamoto M Crystal Structure of OXA-58 with the Substrate-Binding Cleft in a Closed State: Insights into the Mobility and Stability of the OXA-58 Structure. *PLoS One* 2015, 10 (12), e0145869 10.1371/journal.pone.0145869. [PubMed: 26701320]
- (56). Stewart NK; Smith CA; Antunes NT; Toth M; Vakulenko SB Role of the Hydrophobic Bridge in the Carbapenemase Activity of Class D β -Lactamases. *Antimicrob. Agents Chemother.* 2019, 63 (2), 1–13. 10.1128/AAC.02191-18.
- (57). Docquier J-D; Mangani S Structure-Function Relationships of Class D Carbapenemases. *Curr. Drug Targets* 2015, 17 (9), 1061–1071. 10.2174/1389450116666150825115824.
- (58). Gallego L; Rosales I; Fernández E; Bustamante Z; Umaran A; Zabalaga S; Sevillano E Emergence and Clonal Dissemination of Carbapenem-Hydrolysing OXA-58-Producing *Acinetobacter Baumannii* Isolates in Bolivia. *J. Med. Microbiol.* 2011, 61 (1), 80–84. 10.1099/jmm.0.032722-0. [PubMed: 21873380]
- (59). Aleo A; Mamma C; Bonura C; Fasciana T; Abdelaziz MO; El-Domany RA OXA-163-Producing *Klebsiella Pneumoniae* in Cairo, Egypt, in 2009 and 2010. *J. Clin. Microbiol.* 2012, 50 (7), 2489–2491. 10.1128/jcm.06710-11. [PubMed: 22518851]
- (60). Nordmann P; Poirel L; Rodriguez CP; Carrère A; Smayevsky J; Castanheira M; Jones RN OXA-163, an OXA-48-Related Class D β -Lactamase with Extended Activity Toward Expanded-Spectrum Cephalosporins. *Antimicrob. Agents Chemother.* 2011, 55 (6), 2546–2551. 10.1128/aac.00022-11. [PubMed: 21422200]
- (61). Stojanoski V; Chow DC; Fryszczyn B; Hu L; Nordmann P; Poirel L; Sankaran B; Prasad BVV; Palzkill T Structural Basis for Different Substrate Profiles of Two Closely Related Class D β -Lactamases and Their Inhibition by Halogens. *Biochemistry* 2015, 54 (21), 3370–3380. 10.1021/acs.biochem.5b00298. [PubMed: 25938261]
- (62). June CM; Vallier BC; Bonomo RA; Leonard DA; Powers A Structural Origins of Oxacillinase Specificity in Class D β -Lactamases. 2014, 58 (1), 333–341. 10.1128/AAC.01483-13.
- (63). Kobayashi S; Arai S; Hayashi S; Sakaguchi T In Vitro Effects of β -Lactams Combined with β -Lactamase Inhibitors against Methicillin-Resistant *Staphylococcus Aureus*. *Antimicrob. Agents Chemother.* 1989, 33 (3), 331–335. 10.1128/AAC.33.3.331. [PubMed: 2786369]
- (64). Docquier JD; Calderone V; De Luca F; Benvenuti M; Giuliani F; Bellucci L; Tafi A; Nordmann P; Botta M; Rossolini GM; Mangani S Crystal Structure of the OXA-48 β -Lactamase Reveals Mechanistic Diversity among Class D Carbapenemases. *Chem. Biol.* 2009, 16 (5), 540–547. 10.1016/j.chembiol.2009.04.010. [PubMed: 19477418]
- (65). Brosius J; Erfle M; Storella J Spacing of the –10 and –35 Regions in the Tac Promoter. Effect on Its in Vivo Activity. *J. Biol. Chem.* 1985, 260 (6), 3539–3541. [PubMed: 2579077]
- (66). Cox G; Wright GD Intrinsic Antibiotic Resistance: Mechanisms, Origins, Challenges and Solutions. *Int. J. Med. Microbiol.* 2013, 303 (6–7), 287–292. 10.1016/j.ijmm.2013.02.009. [PubMed: 23499305]
- (67). Hiroshi N Prevention of Drug Access to Bacterial Targets: Permeability Barriers and Active Efflux. *Science* (80-.). 1994, 264 (April), 382–388.
- (68). Delcour AH Outer Membrane Permeability and Antibiotic Resistance. *Biochim. Biophys. Acta - Proteins Proteomics* 2009, 1794 (5), 808–816. 10.1016/j.bbapap.2008.11.005.Outer.

- (69). Masi M; Réfregiers M; Pos KM; Pagès JM Mechanisms of Envelope Permeability and Antibiotic Influx and Efflux in Gram-Negative Bacteria. *Nat. Microbiol.* 2017, 2(3). 10.1038/nmicrobiol.2017.1.
- (70). Zgurskaya H; Lopez C; Gnanakaran S Permeability Barrier of Gram-Negative Cell Envelopes and Approaches To Bypass It. *ACS Infect Dis.* 2015, 1 (11), 512–522. 10.1021/acinfecdis.5b00097.Permeability. [PubMed: 26925460]
- (71). Richter MF; Drown BS; Riley AP; Garcia A; Shirai T; Svec RL; Hergenrother PJ Predictive Compound Accumulation Rules Yield a Broad-Spectrum Antibiotic. *Nature* 2017, 545 (7654), 299–304. 10.1038/nature22308. [PubMed: 28489819]
- (72). Goodnow RA; Dumelin CE; Keefe AD DNA-Encoded Chemistry: Enabling the Deeper Sampling of Chemical Space. *Nat. Rev. Drug Discov.* 2017, 16 (2), 131–147. 10.1038/nrd.2016.213. [PubMed: 27932801]
- (73). Sun J; Deng Z; Yan A Bacterial Multidrug Efflux Pumps: Mechanisms, Physiology and Pharmacological Exploitations. *Biochem. Biophys. Res. Commun.* 2014, 453 (2), 254–267. 10.1016/j.bbrc.2014.05.090. [PubMed: 24878531]
- (74). Studier FW; Moffatt BA Use of Bacteriophage T7 RNA Polymerase to Direct Selective High-Level Expression of Cloned Genes. *J. Mol. Biol.* 1986, 189 (1), 113–130. 10.1016/0022-2836(86)90385-2. [PubMed: 3537305]
- (75). Rosenberg AH; Lade BN; Dao-shan C; Lin SW; Dunn JJ; Studier FW Vectors for Selective Expression of Cloned DNAs by T7 RNA Polymerase. *Gene* 1987, 56 (1), 125–135. 10.1016/0378-1119(87)90165-X. [PubMed: 3315856]
- (76). Phillip S; Chen Y Use of T7 RNA Polymerase to Direct Expression of Cloned. *Methods Enzymol.* 1990, 185, 60–89. 10.1109/MSP.2007.273050. [PubMed: 2199796]
- (77). Morrison JF Kinetics of the Reversible Inhibition of Enzyme-Catalysed Reactions by Tight-Binding Inhibitors. *Biochim. Biophys. Acta - Enzymol.* 1969, 185 (2), 269–286. 10.1016/0005-2744(69)90420-3.
- (78). McCoy AJ; Grosse-Kunstleve RW; Adams PD; Winn MD; Storoni LC; Read RJ Phaser Crystallographic Software. *J. Appl. Crystallogr.* 2007, 40 (4), 658–674. 10.1107/S0021889807021206. [PubMed: 19461840]
- (79). Skubák P; Murshudov GN; Pannu NS Direct Incorporation of Experimental Phase Information in Model Refinement. *Acta Crystallogr. Sect. D Biol. Crystallogr.* 2004, 60 (12I), 2196–2201. 10.1107/S0907444904019079. [PubMed: 15572772]
- (80). Adams PD; Afonine PV; Bunkóczi G; Chen VB; Davis IW; Echols N; Headd JJ; Hung LW; Kapral GJ; Grosse-Kunstleve RW; McCoy AJ; Moriarty NW; Oeffner R; Read RJ; Richardson DC; Richardson JS; Terwilliger TC; Zwart PH PHENIX: A Comprehensive Python-Based System for Macromolecular Structure Solution. *Acta Crystallogr. Sect. D Biol. Crystallogr.* 2010, 66 (2), 213–221. 10.1107/S0907444909052925. [PubMed: 20124702]
- (81). Emsley P; Cowtan K Coot: Model-Building Tools for Molecular Graphics. *Acta Crystallogr. Sect. D Biol. Crystallogr.* 2004, 60 (12I), 2126–2132. 10.1107/S0907444904019158. [PubMed: 15572765]
- (82). Chen VB; Arendall WB; Headd JJ; Keedy DA; Immormino RM; Kapral GJ; Murray LW; Richardson JS; Richardson DC MolProbity: All-Atom Structure Validation for Macromolecular Crystallography. *Acta Crystallogr. Sect. D Biol. Crystallogr.* 2010, 66 (1), 12–21. 10.1107/S0907444909042073. [PubMed: 20057044]
- (83). Schrödinger LLC. Schrödinger Suite 2019-1. New York, NY 2019.
- (84). Sastry GM; Adzhigirey M; Day T; Annabhimoju R; Sherman W Protein and Ligand Preparation: Parameters, Protocols, and Influence on Virtual Screening Enrichments. *J. Comput. Aid. Mol. Des* 27, 221–234.
- (85). Olsson MH; Sondergaard CR; Rostkowski M; Jensen JH PROPKA3: Consistent Treatment of Internal and Surface Residues in Empirical PKa Predictions *J. Chem. Theory Comput* 7, 525–537.
- (86). Greenwood JR; Calkins D; Sullivan AP; Shelley JC Towards the Comprehensive, Rapid, and Accurate Prediction of the Favorable Tautomeric States of Drug-like Molecules in Aqueous Solution. *J. Comput. Aided Mol. Des* 24, 591–604. [PubMed: 20354892]

- (87). Shelley JC; Cholleti A; Frye L; Greenwood JR; Timlin MR; Uchimaya M Epik: A Software Program for PKa Prediction and Protonation State Generation for Drug-like Molecules. *J. Comp. Aided Mol. Des* 21, 681–691.
- (88). Halgren TA; Murphy RB; Friesner RA; Beard HS; Frye LL; Pollard WT; Banks JL Glide: A New Approach for Rapid, Accurate Docking and Scoring. 2. Enrichment Factors in Database Screening. *J. Med. Chem* 47, 1750–1759.
- (89). Friesner RA; Murphy RB; Repasky MP; Frye LL; Greenwood JR; Halgren TA; Sanschagrin PC; Mainz DT Extra Precision Glide: Docking and Scoring Incorporating a Model of Hydrophobic Enclosure for Protein-Ligand Complexes *J. Med. Chem* 49, 6177–6196.
- (90). Halgren TA; Murphy RB; Friesner RA; Beard HS; Frye LL; Pollard WT; Banks JL Glide: A New Approach for Rapid, Accurate Docking and Scoring. 2. Enrichment Factors in Database Screening. *J. Med. Chem.* 2004, 47 (7), 1750–1759. 10.1021/jm030644s. [PubMed: 15027866]
- (91). Schrödinger LLC. Schrödinger Release 2019-4: Maestro. New York, NY 2019.
- (92). Sun Z; Mehta SC; Adamski CJ; Gibbs RA; Palzkill T Deep Sequencing of Random Mutant Libraries Reveals the Active Site of the Narrow Specificity CphA Metallo- β -Lactamase Is Fragile to Mutations. *Sci. Rep.* 2016, 6 (5), 1–12. 10.1038/srep33195. [PubMed: 28442746]

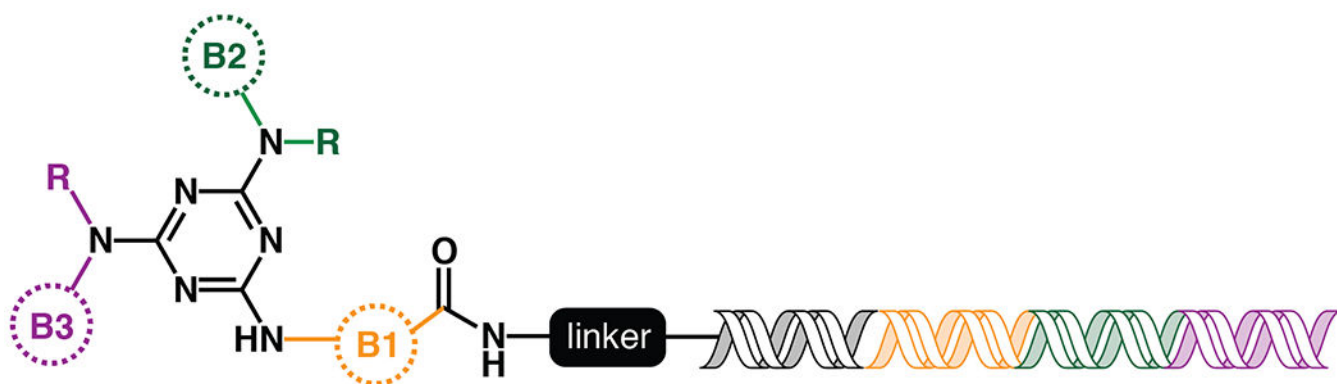


Figure 1. Topology of the DNA-encoded library synthesized and screened against OXA-48. For each library, the colored circles indicate building block 1 (orange), 2 (green) and 3 (purple). The “R” on positions B2 and B3 indicates both primary and secondary amines were added at these positions. The sequences within the DNA tag are color-coded to correspond to which building block it is encoding.

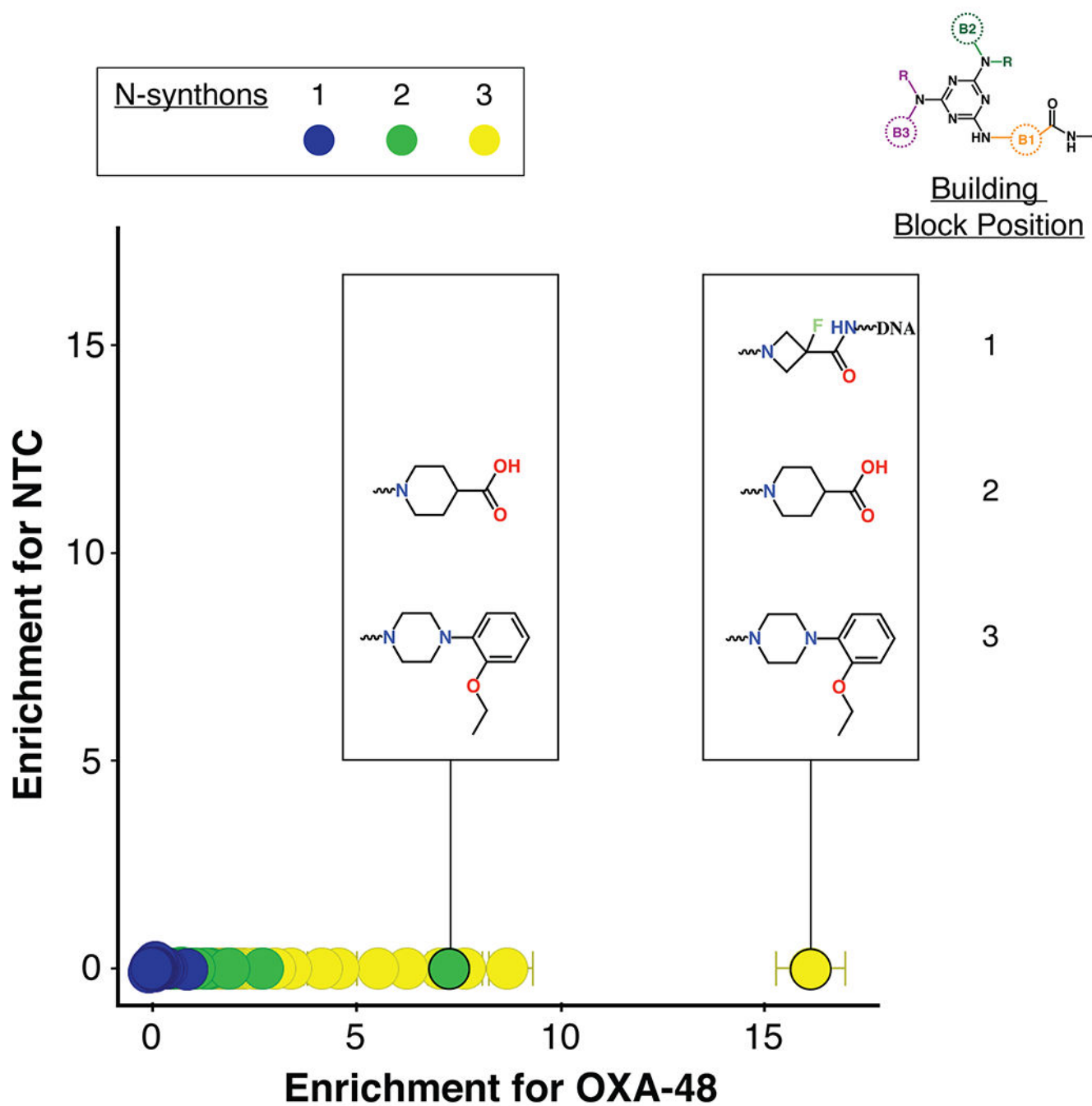


Figure 2. Enrichment plot of triazine DECL compounds for binding to OXA-48 versus the control. Points represent observed *n*-synthons and are color-coded by the number of component building blocks: mono-synthons are blue, di-synthons are green and tri-synthons are yellow. The y-axis is the normalized z-score of enrichment for the non-target control selection versus the x-axis which represents this score for the OXA-48 selection.

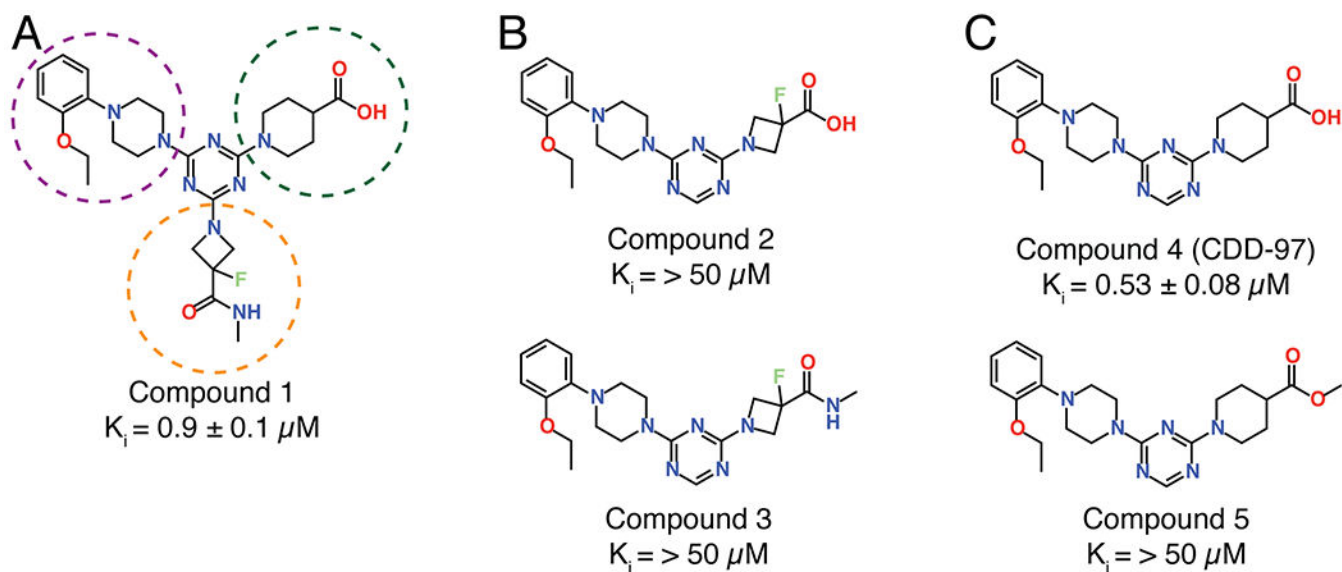


Figure 3.

Compounds designed and synthesized based on the synthons enriched for binding OXA-48 in the DECL screening. Compound 1 represents the most enriched compound in the screen and showed a submicromolar K_i against OXA-48. The building blocks of compound 1 are circled based on the color-coding of building block position shown in Figure 2; orange is building block 1, green is building block 2 and purple is building block 3. To assess the importance of the B1 building block, Compound 2 was created with the acid form of the most enriched cycle 1 building block along with a methylated version (Compound 3), however potency was low for both compounds. CDD-97 (Compound 4) was designed based on the most enriched *di-synthon*. It showed the highest activity with a sub-micromolar K_i . The methylated version (Compound 5) showed low activity revealing the importance of the acid for potency.

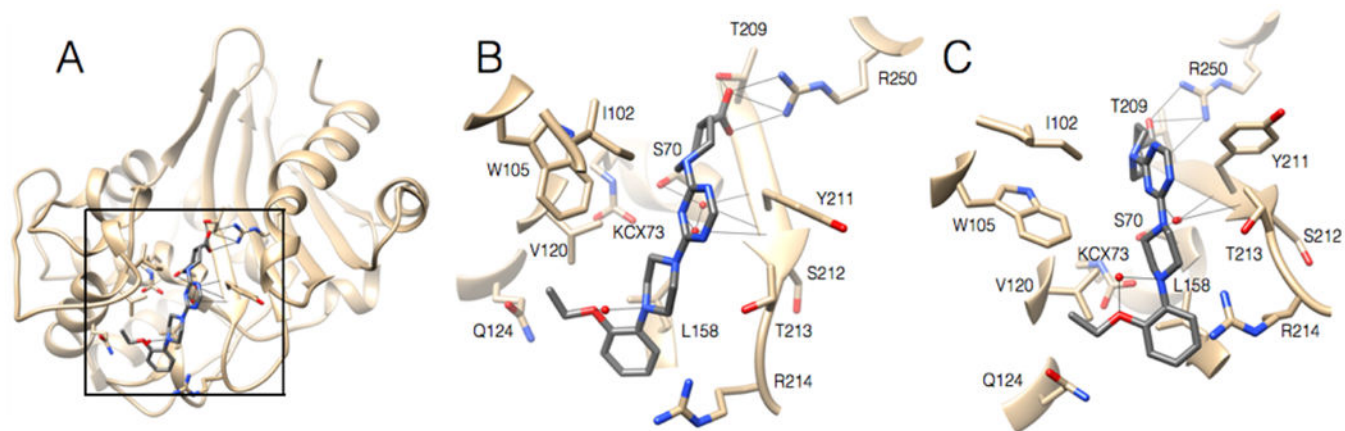


Figure 4.

A. Ribbon diagram of 2.2 Å structure of OXA-48 (tan) bound with CDD-97 (gray). The box indicates the region viewed in 4B and 4C. **B.** Active site region of OXA-48 with CDD-97 shown in gray with nitrogen and oxygen atoms colored in blue and red, respectively. OXA-48 residues are shown as stick models and labeled. **C.** View of OXA-48 with CDD-97 tilted 30 degrees from the position shown in 4B.

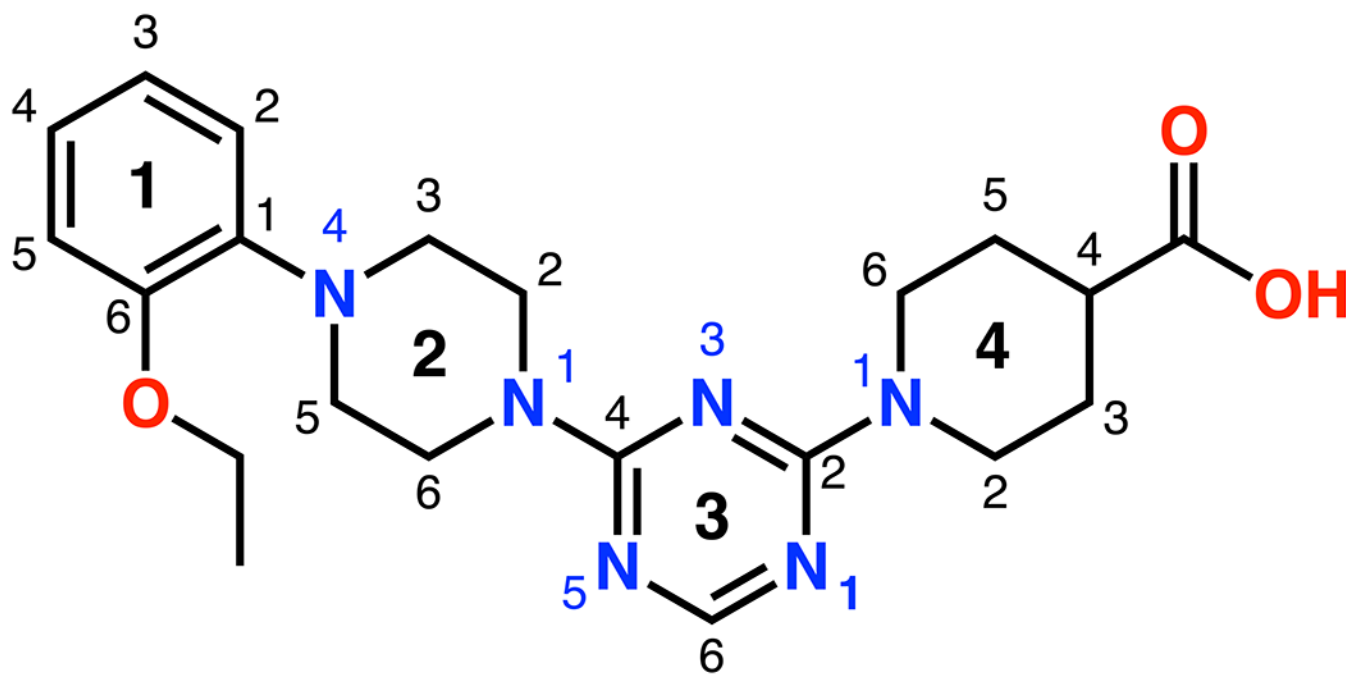


Figure 5.
Schematic showing the ring and atom numbering of the lead compound CDD-97.

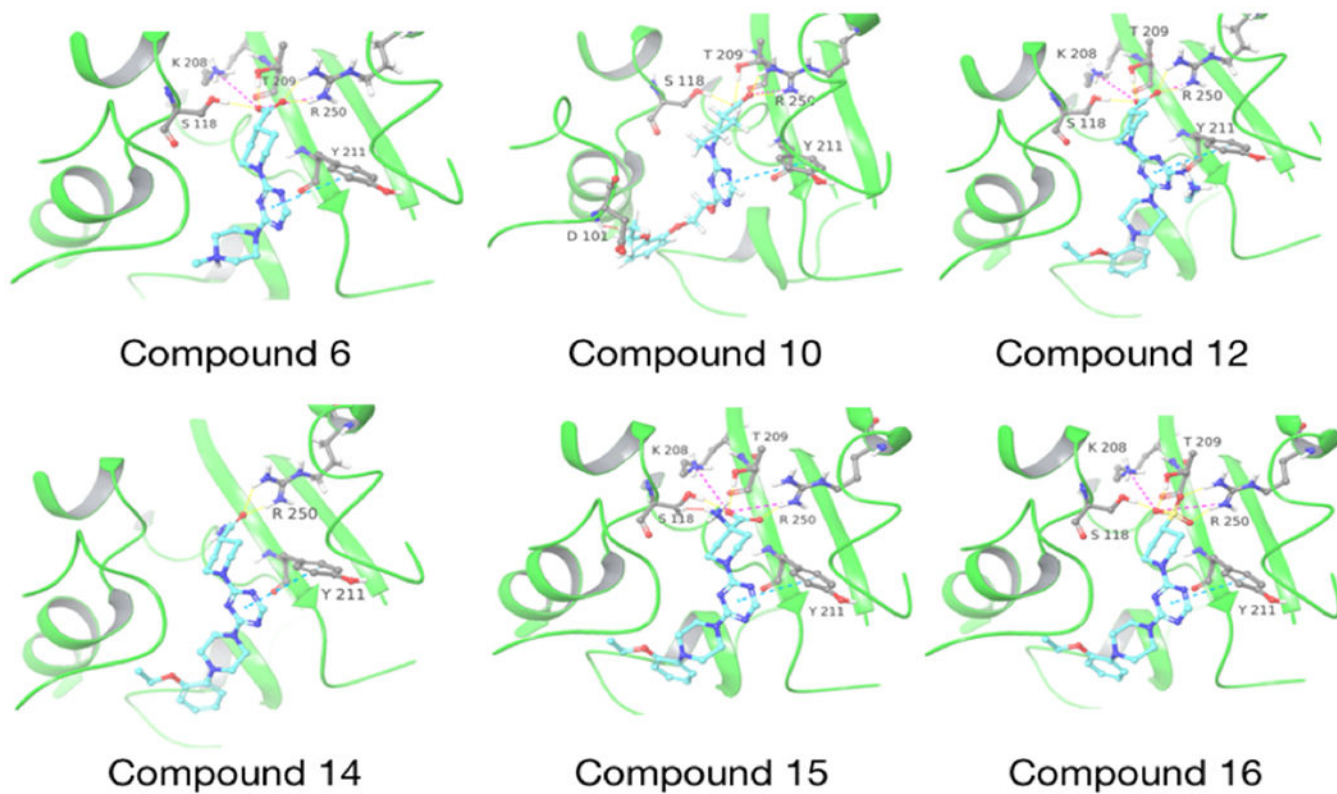


Figure 6. Molecular docking of CDD-97 derivatives in the active site of OXA-48. The docked compound is indicated below each structure. OXA-48 is colored in green and the compounds are colored with carbon-cyan, oxygen-red, nitrogen-blue. Hydrogen bonds are shown as dashed yellow lines, salt bridges are pink dashed lines and clashes are red dashed lines.

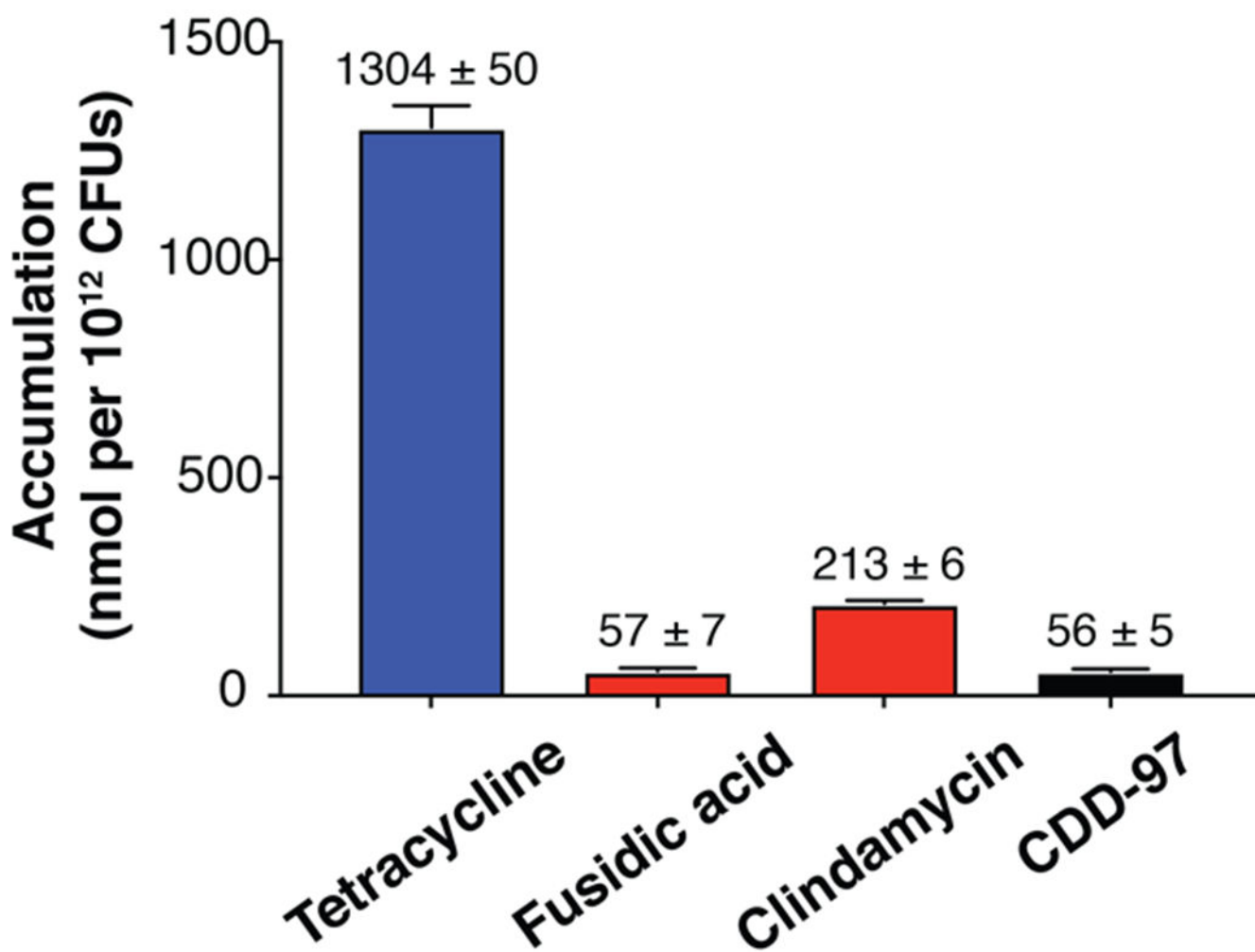
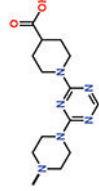

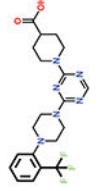
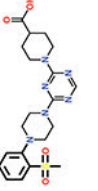
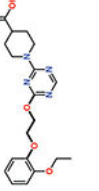

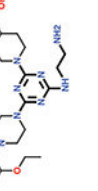
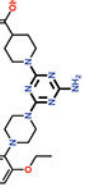
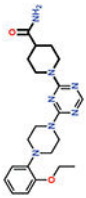
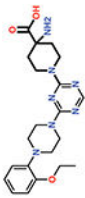
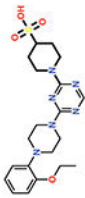


Figure 7. Accumulation of compounds in *E. coli* MG1655. The high accumulating control (tetracycline) is depicted in blue, and the low accumulating controls (clindamycin and fusidic acid) are in red. CDD-97 is shown in black. The number above each column indicates the accumulation value of the given sample.

Table 1. Inhibition of CDD-97 and CDD-97 derivatives for structure-activity relationship studies (modified portion of derivatives is in bold).

Compound I.D.	Structure	K _i (μM)
6		> 50
7		0.76 ± 0.03
8		1.7 ± 0.3
9		2.2 ± 0.2
10		18.8 ± 2.5
11		7.8 ± 0.1
12		0.84 ± 0.03
13		0.61 ± 0.02

Compound I.D.	Structure	K _i (μM)
14		> 50
15		29 ± 4
16		0.26 ± 0.04

Author Manuscript

Author Manuscript

Author Manuscript

Author Manuscript

Table 2.Inhibition constants (K_i) for CDD-97 with various OXA β -lactamases.

Enzyme	Sequence Identity (%)	CDD-97 K_i (μ M)
OXA-48	100.0	0.53 ± 0.08
OXA-10	49.4	61 ± 27
OXA-24	36.1	14 ± 1
OXA-58	36.2	45 ± 0.8
OXA-163	97.9	0.44 ± 0.02

Author Manuscript

Author Manuscript

Author Manuscript

Author Manuscript

Table 3.

Minimum inhibitory concentrations (MICs) of ampicillin (AMP) and imipenem (IMP) against *E. coli* MG1655_{OXA-48} with increasing concentrations of CDD-97 and avibactam.

	MIC ($\mu\text{g/mL}$)	
	AMP	IMP
0	512	0.625
4	1024	0.625
8	512	0.3125
16	512	0.3125
32	512	0.3125
64	512	0.3125
128	512	0.3125
256	512	0.625
[CDD-97] ($\mu\text{g/mL}$)		
	MIC ($\mu\text{g/mL}$)	
	AMP	IMP
0	512	0.625
0.125	256	0.3125
0.25	128	0.3125
0.5	64	0.1563
1	32	0.1563
2	16	0.1563
4	4	0.0781
[Avibactam] ($\mu\text{g/mL}$)		